Astron. Astrophys. 362, 9–18 (2000)

ASTRONOMY AND ASTROPHYSICS

Hα emitting galaxies and the cosmic star formation rate at z $\simeq$ 2.2*

A.F.M. Moorwood[1], **P.P. van der Werf**[2], **J.G. Cuby**[3], **and E. Oliva**[4]

[1] European Southern Observatory, Karl-Schwarzschild-Strasse 2, 85748 Garching, Germany (amoor@eso.org)
[2] Leiden Observatory, P.O Box 9513, 2300 RA Leiden, The Netherlands
[3] European Southern Observatory, Alonso de Cordova 3107, Santiago, Chile
[4] Osservatorio Astrofisico di Arcetri, Largo E. Fermi 5, 50125 Firenze, Italy

Received 3 July 2000 / Accepted 9 August 2000

Abstract. An infrared imaging survey in narrow band filters around 2.1 μm has yielded $\sim$ 10 candidate Hα emitting galaxies at z $\simeq$ 2.2 of which 6 have been subsequently confirmed spectroscopically with ISAAC at the ESO VLT. The survey reached a limiting line flux of $\sim$ 5x10^{-17} erg cm^{-2} s^{-1} and covered 100 arcmin^2 including the Hubble Deep Field South (HDFS) WFPC2 and STIS fields. This is the largest spectroscopically confirmed sample of high redshift galaxies selected by narrow band infrared imaging. None of the objects falls within the areas of the deep HST images but some are visible in the WFPC2 flanking fields and the ESO Imaging Survey (EIS) Deep images of HDFS. Only one of the objects observed by HST appears to be an interacting system. Absence of [NII]$\lambda\lambda$6548,6584 line emission in the spectra is consistent with them being high ionization and/or low metallicity systems. The observed velocity dispersions imply masses of typically 10^{10}M$\odot$ and a rotation curve obtained for one galaxy yields an inclination corrected rotational velocity of $\simeq$ 140 km s^{-1} at 3 kpc which is within the range of nearby disk galaxies.The absolute B magnitude of this galaxy lies 3 magnitudes above the local Tully-Fisher relationship. Star formation rates of the individual galaxies derived from the Hα fluxes are 20–35 M$\odot$ yr^{-1} without any correction for extinction whereas SFRs derived from the rest frame UV continuum fluxes of the same galaxies are up to a factor of 4 lower - consistent with lower extinction to Hα. Comparison with the HST NICMOS grism Hα survey of Yan et al. (1999) reveals little or no evolution in the Hα luminosity function between z $\sim$ 1.3 and 2.2. The inferred star formation rate density of 0.12 M$\odot$ Mpc^{-3} yr^{-1} is also equal to that most recently estimated from the UV continuum fluxes of galaxies at z $\simeq$ 3–4.5 by Steidel et al. (1999). Spectroscopy covering Hβ and [OIII]$\lambda\lambda$4959,5007 is planned to gain further insight into the extinction and metal abundance in these galaxies.

Key words: galaxies: evolution – galaxies: distances and redshifts – galaxies: formation – galaxies: starburst – cosmology: early Universe

Send offprint requests to: A. Moorwood

* Based on observations collected at the European Southern Observatories on La Silla and Paranal, Chile. Also based on data from the ESO Imaging Survey and HST archives.

1. Introduction

Knowledge of both the global star formation history of the Universe and the nature of individual star forming galaxies at high redshift are essential to our understanding of galaxy formation and evolution. Out to z $\simeq$ 1 the star formation rate density is observed to have increased substantially. The most commonly referenced study, based on star formation rates inferred from the rest frame UV continua of CFRS galaxies, yields a factor $\simeq$ 15 increase, equivalent to luminosity evolution of (1+z)^4 (Lilly et al. 1996). At higher redshifts, the major breakthrough came with the detection of large numbers of the so-called Lyman Break Galaxies at z$\geq$3. These objects are recognizable in deep UV-visible broadband images by their absence of continuum flux due to absorption at wavelengths shorter than the Lyman limit. In a seminal contribution to the field, Madau et al. (1996) combined star formation rates derived from the UV continua of these galaxies with those at lower redshifts to produce a plot of star formation rate density (SFRD) versus z which implied a decline at $z \geq 3$ relative to $z = 1$ and suggestive of a possible peak at $z \simeq 2$. The most recent versions of this diagram which take into account extinction, however, yield both higher values of the SFRD and suggest that it may actually be rather flat from $z = 1$ to possibly beyond $z = 4$ (Steidel et al. 1999).

We present here the results of a programme whose objectives were to establish a sample of star forming galaxies at $z \simeq 2$ both for spectroscopic follow-up studies and to determine the SFRD. Because of the difficulty of finding and spectroscopically confirming galaxies at this redshift in the visible we adopted the technique of narrowband infrared imaging around 2.1 μm to survey for Hα line emission at z$\simeq$2.2. As a star formation tracer this line also has advantages relative to the UV continuum in that it is more directly related to the youngest hot stars, and hence the current star formation activity, and is expected to suffer lower extinction. The extinction can also be estimated by measuring the Balmer decrement. Spectroscopic measurements of Hα in selected CFRS galaxies (Glazebrook et al. 1999), Hα and Hβ in Lyman Break galaxies (Pettini et al. 1998) and results presented here do in fact yield SFRs which are a factor of a few higher than derived from the UV continuum without extinction correction. For spectroscopic follow-up, narrow band filter imaging also provides the advantage that the wavelength of the redshifted Hα

line can be selected to fall in a clean region between the forest of OH sky lines which hampers near infrared spectroscopy. The highest redshift accessible is $\simeq$ 2.5 beyond which the Hα line is redshifted out of the clean part of the K band window and the sensitivity of groundbased observations falls dramatically due to the increasing thermal background.

At lower redshifts, the Hα luminosity function at $z = 0$ has been measured by Gallego et al. (1995) and at z $\simeq$0.2 by Tresse & Maddox (1998). A spectroscopic grism survey for Hα at z = 0.6–1.8 has also been conducted with NICMOS on the HST and has yielded the Hα luminosity function and SFRD corresponding to a mean redshift of $\simeq$ 1.3 (Yan et al. 1999). In principle, therefore, it is now possible to trace the star formation history from z = 0 to 2.5 using Hα emission alone.

Although the advent of large format infrared arrays has made high z Hα surveys feasible, the tradeoff between sensitivity and area coverage remains a critical issue and one which is dependent on the scientific aim. The largest area survey to date remains that of Thompson et al. (1996) who targeted emission at the redshifts of selected quasars over a total area of 276 arcmin^2 to a 3σ flux limit of $\simeq$ 3.5x10^{-16} erg s^{-1} cm^{-2}. Only one candidate object at z = 2.43 was detected and later confirmed spectroscopically by Beckwith et al. (1998). Several surveys have subsequently gone deeper over smaller areas and have detected more candidates but predominantly associated with targeted absorption line systems which are not representative of the SFRD on large scales (Mannucci et al. 1998, Teplitz et al. 1998, van der Werf et al. 2000). These surveys have been mostly conducted in the K band to target z $\geq$ 2 galaxies and, to our knowledge, none of the candidates has yet been confirmed spectroscopically. Most recently, however, deep 2.12 μm imaging of the Hubble Deep Field North has been used to measure Hα in two and [OIII]$\lambda\lambda$4959,5007in another two galaxies with known spectroscopic redshifts (Iwamuro et al. 2000). Their deep 2x2$'$ image reached a 3σ flux limit of 3.4x10^{-17} erg cm^{-2} s^{-1} and the lines are identified as Hα in two of the objects and [OIII]λ5007 in the other two.

The project described here started with an infrared imaging survey in narrow band filters around 2.1 μm conducted with SOFI (Moorwood et al. 1998) at the ESO NTT telescope. It reached 3σ flux limits of $\simeq$ 5–12 x 10^{-17} erg cm^{-2} s^{-1} over a total area of $\simeq$ 100 sq. arcmin including the WFPC2 and STIS fields in the Hubble Deep Field South (Williams et al. 2000). Apart from the slightly higher redshift quasar in the STIS field there are no known redshift 'markers' close to our target redshift and we therefore believe our results to be representative of the field galaxy population at $z \simeq 2.2$. Spectroscopic confirmation of most of the best candidate emission line objects obtained subsequently with ISAAC at the VLT (Moorwood et al. 1999) has demonstrated the validity of the survey technique and also provided additional insight into the nature of the galaxies detected.

We describe here both the imaging and spectroscopic observations in Sect. 2; present the results, together with additional groundbased and HST data, in Sect. 3; discuss the possible nature of these objects and derive the star formation rate density at z = 2.2 in Sect. 4 and summarize our conclusions in Sect. 5.

Mainly for ease of comparison with published results we have adopted a cosmology with H$_0$ = 50 km s^{-1} Mpc^{-1} and q$_0$ = 0.5 throughout.

Table 1. The SOFI survey fields

Field	$\lambda(\mu m)$	z	Δz	Flux[a]	Area[b]	Vol[c]
WFPC2	2.09	2.18	0.03	4.8	18.9	1426
WFPC2	2.12	2.23	0.043	6.2	20.3	2194
STIS	2.09	2.18	0.03	9	18	1356
STIS	2.12	2.23	0.043	8	19	2055
Blank	2.09	2.18	0.03	12	20.6	1557

[a] 3σ flux limit in units of 10^{-17} erg cm^{-2} s^{-1}
[b] in arcmin^2
[c] co-moving Mpc^3

2. Observations

2.1. Infrared imaging survey

SOFI, the infrared imager/spectrometer at the ESO NTT telescope (Moorwood et al. 1998) was used in August 1998 to conduct the narrow-band filter search for Hα emitting galaxies at z $\simeq$ 2.2. This instrument is equipped with a 1024x1024 pixel Rockwell 'Hawaii' array detector which covers a field of view of nearly 5x5 arcmin on the sky with pixels of 0.29$''$ in its large field imaging mode. Three survey fields of this size were selected - one each centred on (but larger than) the WFPC2 and STIS fields in the Hubble Deep Field South and one on an anonymous field about 30^o away which was selected to be devoid of bright objects on the DSS. The nominal J2000 field centers were WFPC2: 22 32 56.2, -60 33 02.7; STIS: 22 33 37.7, -60 33 29 and Blank: 20 50 00, -67 50 00. All three fields were observed in both a 1% FWHM filter centred at 2.09 μm, in a region of low OH background emission, and the broad-band Ks (2.16 μm) filter. The STIS and WFPC2 fields were additionally observed in a 1.3% filter centred at 2.12 μm.

All images were taken using the 'autojitter' mode with the telescope being offset by random amounts of up to 20$''$ between individual exposures of typically 6x30 s and 6x10 s in the narrow and broadband Ks filters respectively. Total exposures were 4–6hrs in the narrow and $\simeq$ 1hr in the Ks filter yielding 3 σ line flux detection limits of 5–12x10^{-17} erg s^{-1} cm^{-2} in the different fields. The seeing was close to 1$''$ for all the observations. Allowing for losses at the field edges due to the jitter technique our survey covered 40 sq. arcmin (4200 Mpc^3 co-moving) at z = 2.24 and 60 sq. arcmin (4500 Mpc^3 co-moving) at z = 2.18. Table 1 summarizes the flux limits, areas and volumes surveyed in the SOFI fields.

2.2. ISAAC spectroscopy

Infrared spectra around 2.1 μm of all 8 candidate Hα emitters detected at $\geq 3\sigma$ plus 3 with s/n in the range 2–3 were ob-

tained with ISAAC (Moorwood et al. 1999) at the ESO VLT in June/July 1999. Observations were made using the SW Rockwell 1024x1024 pixel Hawaii array and the medium resolution grating whose resolving power x slit width product is about 2500 at the wavelengths observed. As the seeing was typically only around 1–1.5″ the 2″ slit was in fact used in all cases except for the simultaneous observation of two galaxies with the 1″ slit when the seeing was around 0.6″. The target galaxies were acquired using the imaging mode of ISAAC. Because of their faintness, advantage was taken of the long (2′) slit to accurately centre the targets by angular offsetting relative to two nearby brighter objects in the field. In each case, the first step was to centre the two reference objects in the slit. Using the telescope rotator, the field was then rotated by the measured angular offset of the target galaxy relative to the line between the two reference objects in the SOFI images to avoid errors due to uncertainties in the exact scale. The telescope was then offset to centre one of the reference objects as well as the target galaxy in the slit. This technique facilitates location of the faint object spectrum in the 2D sky subtracted frames and provides a check on the telescope tracking and flexure during the observations. In two cases, it was actually possible to centre two target objects plus a reference simultaneously in the slit. Each observation comprised four 15min on-chip integrations with the object moved between exposures by 5–10″ along the slit in an ABBA sequence. Fig. 1 shows the reduced 2D, sky subtracted, spectrum of 338.165–60.518 plus the reference galaxy above obtained by spatially shifting the A-B and B-A frames by the offset and then averaging. This yields a positive object spectrum and 2 negative ones of half the amplitude on either side. This technique not only yields good sky subtraction but also allows faint lines to be distinguished from cosmetic detector effects which only yield a positive and one negative spectrum.1D spectral traces integrated over the spatial extent of the objects were extracted using standard MIDAS routines. Flux calibration has been derived from observations of the standard star HD216009 made with both the 1″ and 2″ slits which yielded closely similar fluxes.

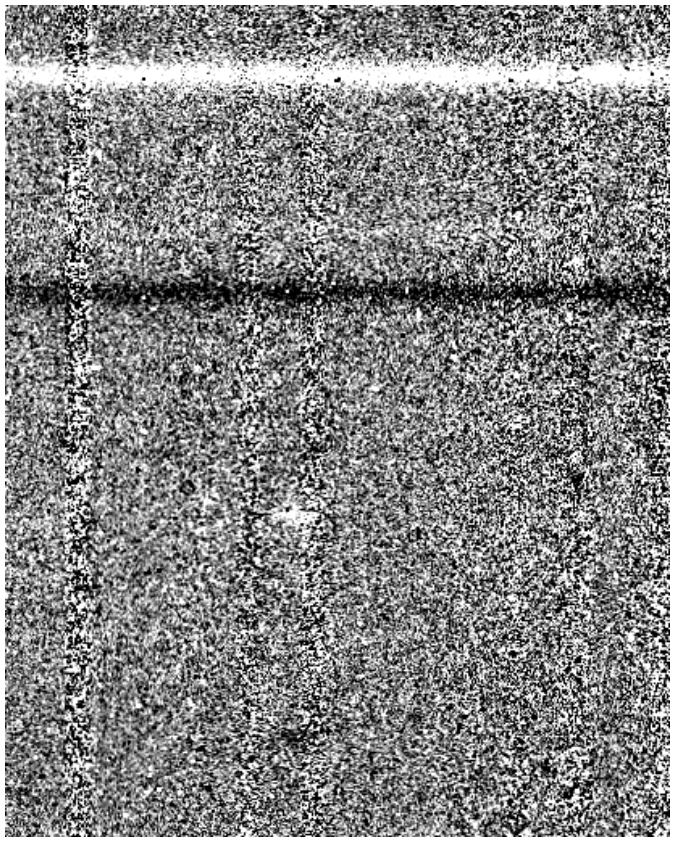

Fig. 1. Sky subtracted 2D ISAAC spectrum of 338.165–60.518 and the reference galaxy above. Emission is only detected at the position of the Hα line in the programme galaxy whereas the reference galaxy is much brighter in the continuum. Note the positive and 2 negative images due to the sky subtraction technique used and the increased shot noise at the position of the OH sky lines.

3. Results

3.1. SOFI survey

Fig. 2 shows the narrow 2.09 μm (upper) and Ks broad band SOFI images centred on the WFPC2 field as an example. Squares identify the Hα emitting candidates subsequently confirmed spectroscopically. Catalogues of the objects in all 5 survey fields were made using SExtractor (Bertin & Arnouts 1996).Candidate line emitting objects were then selected on the basis of their excess narrow versus broad band flux in plots of m_{nb}-m_k vs m_{nb}. Fig. 3 is the plot for the WFPC 2.09 μm field showing the loci for flux excess at the 1,2 and 3σ level as well as the limits on equivalent width. Due to the area coverage and depth reached the large number of galaxies detected in total means that the *trumpet* shaped region occupied by non-line emitting galaxies is well defined by the data. Several candidates exhibiting excess emission are clearly visible. Most of the candidates in fact were found in this field due to the lower flux limit achieved relative to the others and/or possibly clustering effects.

Although the 2.09 μm filter corresponds to Hα at the highest redshift of several absorption systems along the line of sight to the STIS quasar no candidates were actually detected in this filter/field combination implying that our data are not affected by clustering associated with this object.

Table 2 lists the candidates detected at $\geq 3\sigma$ plus those with lower s/n ratios for which ISAAC spectra were obtained. Also given are the Ks magnitudes and Hα line fluxes measured both in the narrow band filter and from the spectra. Agreement between the photometric and spectroscopic line fluxes is actually excellent if account is taken of the fact that the largest discrepancies are due to those lines which did not fall close to the central wavelength of the narrow band filter.

3.2. Colours and morphology

Most, but not all, of our candidates fall in the ESO SUSI2/SOFI EIS Deep fields (http://www.eso.org/science/eis/). Complete UBVRIJHKs photometry is available for a few and the most interesting result is that 3 of the Hα emitting galaxies show

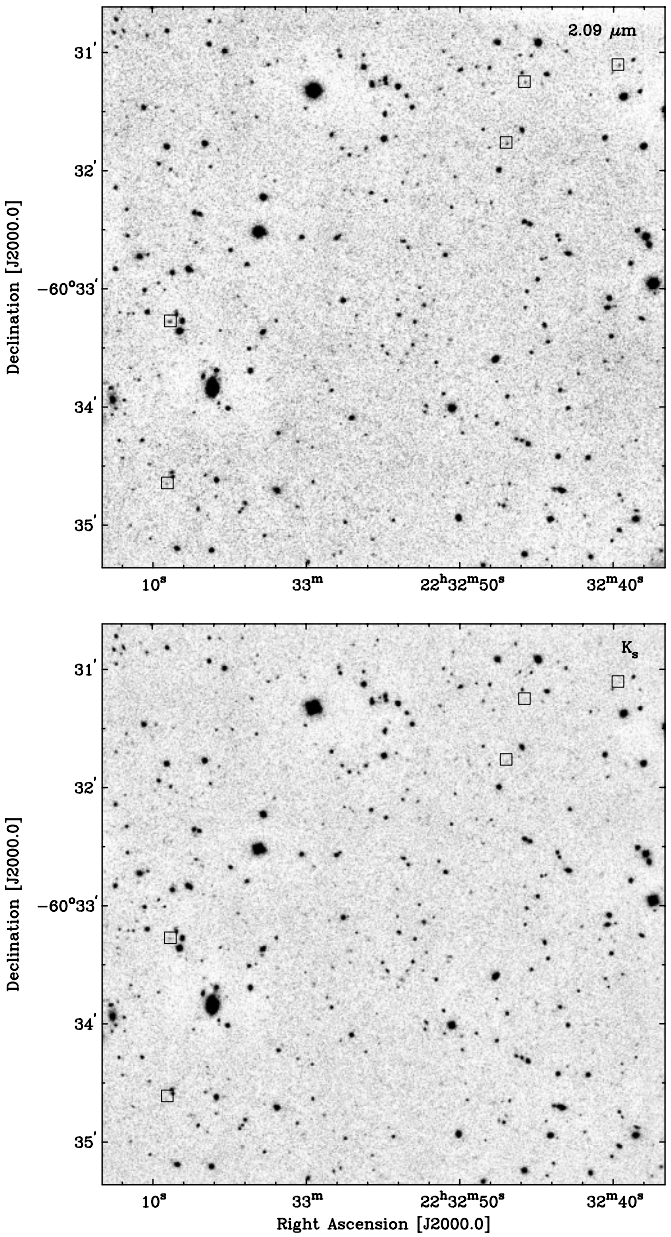

Fig. 2. 2.09 μm narrow (upper panel) and Ks broad band band images centred on the WFPC2 field. Field is 5x5′ with N at the top and E to the left. The squares identifiy the Hα emitting candidates confirmed spectroscopically.

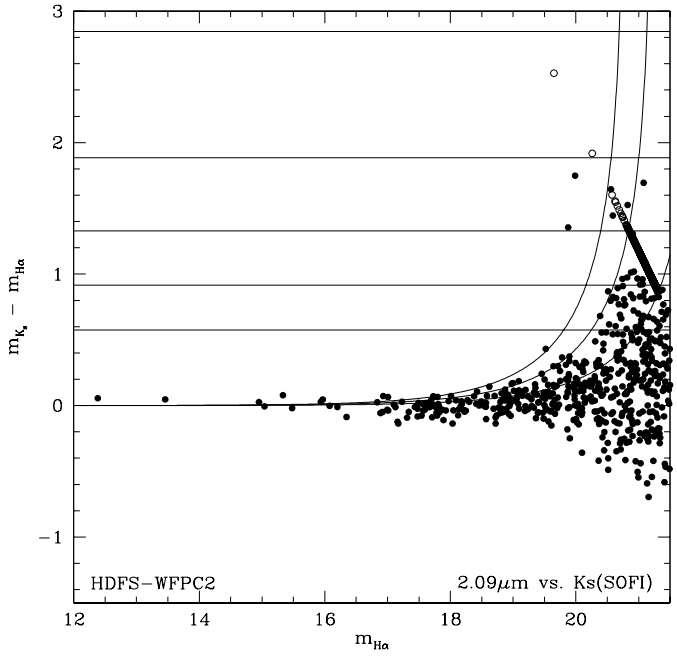

Fig. 3. m(Ks)-m(Hα) vs m(Hα) for the 2.09 μm survey centred on the WFPC2 HDFS field. The solid lines represent the 1,2 and 3σ line detection limits and the horizontal lines correspond to rest equivalent widths of 50, 100, 200 500 Å and infinity. The open symbols represent sources only detected in the narrow band filter and are therefore lower limits.

Table 2. SOFI candidate/confirmed Hα emitters

Field	$\lambda(\mu m)$	Object	Ks	s/n[a]	Hα[b]
WFPC	2.09	338.165–60.518	21.7	5	7.8/9
		338.191–60.521	–	4	7.6/9
		338.193–60.527	–	2.8	$4.4/\leq 5$
		338.196–60.529	21.2	5	7.7/10
		338.287–60.555	20.7	5	8.1/9
		338.288–60.577	21.4	2.1	3.3/8
		338.290–60.572	21.3	2.6	$4.6/\leq 5$
WFPC	2.12	338.300–60.539	–	3.2	$7.3/\leq 5$
STIS	2.12	338.366–60.547	21.2	5	14.6/13
		338.382–60.523	20.5	3.4	$8.9/\leq 5$
		338.407–60.558[c]	14.8	600	960/–
Blank	2.09	306.300–67.863	–	5	$26/\leq 5$

[a] detection significance in imaging survey
[b] 10^{-17} erg cm^{-2} s^{-1} in NB filter/spectra
[c] quasar in STIS field

extremely red U-B colours ($\geq$2 mag.) which are presumably due to Lyman forest absorption at the survey redshift of 2.2. This provides support for the Hα detections but also implies that these objects could have been detected in a photometric redshift survey. Images of 338.196–60.529 are shown in Fig. 4. Note that the galaxy is visible in the B to I bands but not U and is bright in the NB 2.09 μm filter whereas it is not detected in the NB 2.12 μm filter and only barely in Ks.

All of the candidate line emitting objects in our 5x5′ images fall outside the smaller deep HDFS fields observed with WFPC2 and STIS although some were observed in the WFPC2 flanking fields (http://www.stsci.edu/ftp/science/hdfsouth/hdfs.html). The F814W image of 338.287–60.555 shown in Fig. 5 is of particular interest and suggests that this is an interacting system with 2 or 3 components within $\simeq 1''$ (8 kpc). This object is also the most diffuse of the sample in the infrared narrow band and spectral images. It appears to be the only such case within our sample. The F814W image of 338.288–60.577 shown in Fig. 6 is also of interest as this object is the only one in which we see a rotation curve in Hα. The HST image shows a single galaxy whose major axis is roughly N-S in

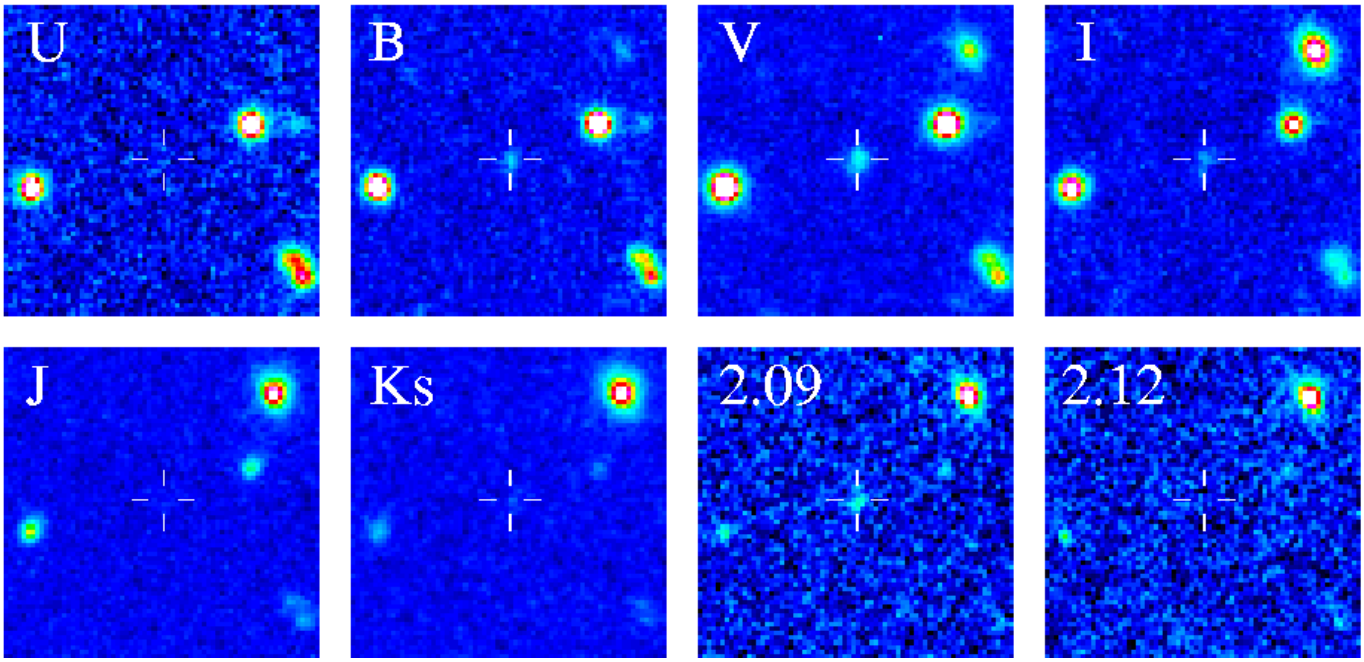

Fig. 4. Images of a 20x20″ region centred on 338.196–60.529. The U,B,V,I images were obtained in the EIS Deep programme and the J, Ks NB 2.09 μm and NB 2.12 μm images in the present work. Note that the object at the centre is well detected in B to I but not U and, relative to the other objects in the field, is much brighter in the NB2.09 μm than the Ks filter and undetected in the NB 21.12 μm filter. This appearance is characteristic of a galaxy at z=2.18 suffering Lyman forest absorption in the U band and with a strong, redshifted Hα emission line falling within the NB 2.09 μm filter.

which case it is within about 10° of the slit orientation used. The other objects for which F814W images are available, 338.165–60.518, 338.191–60.521,338.196–60.529 show no particularly interesting morphological structure but their fluxes allow the comparison made below of SFRs derived from the rest frame UV continuum and Hα.

3.3. ISAAC spectroscopy

Spectra of the 6 objects (the STIS quasar has been excluded) showing a clear emission line at the expected wavelength are shown in Fig. 7. The ratio of spectroscopically confirmed to total Hα candidates as a function of their s/n in the imaging survey are 5/6 at $\geq 4\sigma$, 5/8 at $\geq 3\sigma$; and 1/3 at $\leq 3\sigma$. In the last group, although only detected at 2σ in the survey, the spectroscopically measured flux of 338.288–60.577 turned out to be higher because its redshift places the line away from the centre of the NB filter. This object was also observed under the best seeing conditions ($\simeq$0.6″) with the 1″ slit and is the only one which exhibits a clear rotation curve. For the other two s/n ≤ 3 sources it appears that the flux sensitivity reached in the spectra might have been insufficient even if these objects are real. This illustrates the difficulty of establishing completeness at the survey limit. Non confirmation of 306.300–67.536, the brightest of those detected at $\geq 4\sigma$ is potentially the most surprising except that it was not detected in the Ks filter and therefore may be spurious. In the case of non-detections there also remain the possibilities of poor centering or that the line is coincident in position with an atmospheric OH line.

The first and most important conclusion from the spectra is that most of the objects detected at $\geq 4\sigma$ in our imaging survey do actually exhibit an emission line at the correct wavelength. It is important to stress this as very few of the infrared objects detected by this technique previously have been spectroscopically confirmed. In principle, a problem of identification remains as only a single line appears in the spectra. On the other hand, this eliminates the most serious alternative to Hα which is [OIII]$\lambda\lambda$4959,5007. The 4959/5007 ratio of the [OIII] doublet is 0.33 so both lines should be visible at the s/n achieved.The only other serious possibility is [OII]λ3727 but this is both intrinsically fainter than Hα and the objects would have to be at $z = 4.6$. This is also a doublet with almost equally intense components although they would only be marginally resolvable in our spectra. A marginal detection of redhifted [OIII]λ5007 obtained in a short H band spectrum of 338.366–60.547 is also consistent with the line at 2.1 μm being Hα.

If, as appears most likely, the detected lines are all Hα then it is of interest that [NII]$\lambda\lambda$6548,6584, whose expected positions are marked on Fig. 7 are not detected. The [NII]/Hα ratio shows wide variations with galaxy type, ionization degree, abundance etc. The most commonly used diagnostic diagram for emission line galaxies is the plot of [OIII]λ5007/Hβ versus [NII]λ6584/Hα. Based on this diagram in Gallego et al. (1997), low [NII]λ6584/Hα ratios are characteristic of high ionization, low metallicity systems. For a sample of Lyman Break galaxies at z $\sim$ 3 observed with NIRSPEC and ISAAC (Pettini 2000) the [OIII]λ5007/Hβ ratios are typically ≥ 3 which corresponds to the same part of the diagram and would imply [NII]λ6584/Hα

Table 3. Derived quantities from ISAAC spectra.

Field	Source	z	Slit($''$)	Hα[a]	L(Hα)[b]	SFR($M_\odot/yr$)	FWHM(obs.)[c]	σ_v[c]
WFPC209	338.165–60.518	2.183	2	9 ± 0.5	3.066	24.2	479	175
	338.191–60.521	2.185	2	9 ± 1.2	3.07	24.3	151	–
	338.196–60.529	2.178	2	10 ± 1	3.39	26.8	202	–
	338.287–60.555	2.188	2	9 ± 0.7	3.08	24.3	350	≥ 108
	338.288–60.577	2.192	1	8 ± 0.5	2.75	21.74	301	117
STIS212	338.366–60.547	2.221	2	13 ± 1.7	4.61	36.42	273	≥ 50

[a] 10^{-17} erg cm^{-2} s^{-1} [b] 10^{42} erg s^{-1} [c] km s^{-1}

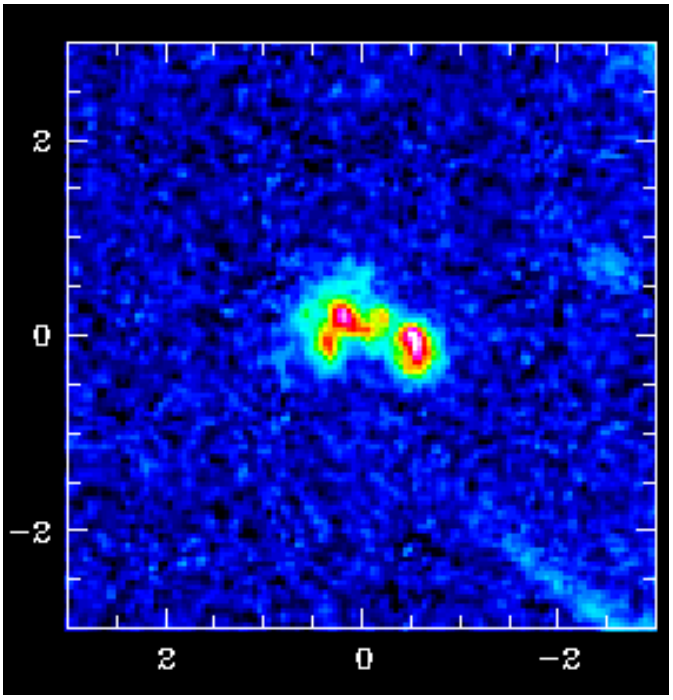

Fig. 5. WFPC2 HDFS flanking field F814W image of 338.287–60.555. Scale is in arcsec..

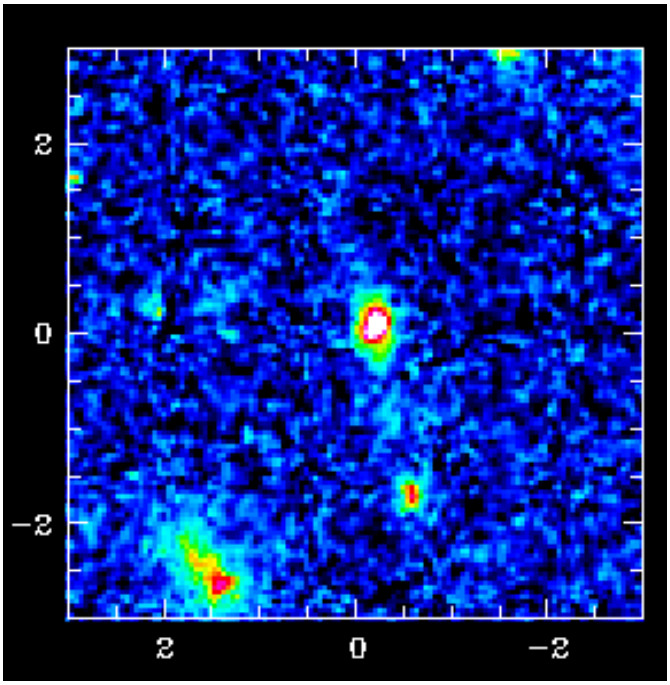

Fig. 6. WFPC2 HDFS flanking field F814W image of 338.288–60.577. Scale is in arcsec..

≤ 0.1 if these objects are of similar nature. Absence of the [NII] lines in our relatively low s/n spectra is therefore not particularly surprising and can actually be taken as evidence for the high ionization degree and/or low metal abundances which is to be expected at this redshift.

4. Discussion

4.1. Star formation rates

Star formation rates for the spectroscopically confirmed galaxies have been computed using the formula SFR($M_\odot$/yr) = 7.9x10^{-42} L(Hα)(erg s^{-1}) from Kennicutt (1998) which is appropriate for continuous star formation and a Salpeter IMF extending from 0.1–100$M_\odot$. The values of 20–35 $M_\odot$/yr, reported in Table 3, are higher than found in the disks of late type spirals but lower than in the most extreme nearby starburst galaxies. As no extinction correction has been applied to the Hα fluxes, however, the actual values could be higher. The canonical value is $A_{H\alpha}$ = 1.1 mag for nearby spirals (Kennicutt 1983) but increases to $\simeq$ 5–40 mag. in Ultraluminous Infrared Galaxies which are believed to harbour the most powerful starbursts (Genzel et al. 1998). Unfortunately, spectra around Hβ which would allow an estimate of the extinction from the Balmer decrement could not be obtained within the available telescope time. For some of our objects, however, we have been able to extract I band fluxes from HST (WFPC2 F814W) observations of the HDFS flanking fields and EIS Deep images obtained with the ESO NTT. The flux conversions used were as given in the respective file headers. As the wavelength corresponds to $\simeq$ 2500 Å in the rest frame it is possible for these galaxies to compute the SFR also from their rest frame UV continua using the analogous formula SFR = 1.4x10^{-28} L(1500–2800 Å)(erg s^{-1}Hz^{-1}) from Kennicutt (1998) which is based on the same model assumptions. This is done in Table 4 where it can be seen that the SFRs deduced from Hα are higher on average by a factor $\simeq$ 2. For the two Hα emitting objects detected in HDFN, Iwamuro et al. (2000) also derive SFRs which are almost a factor of 2 higher

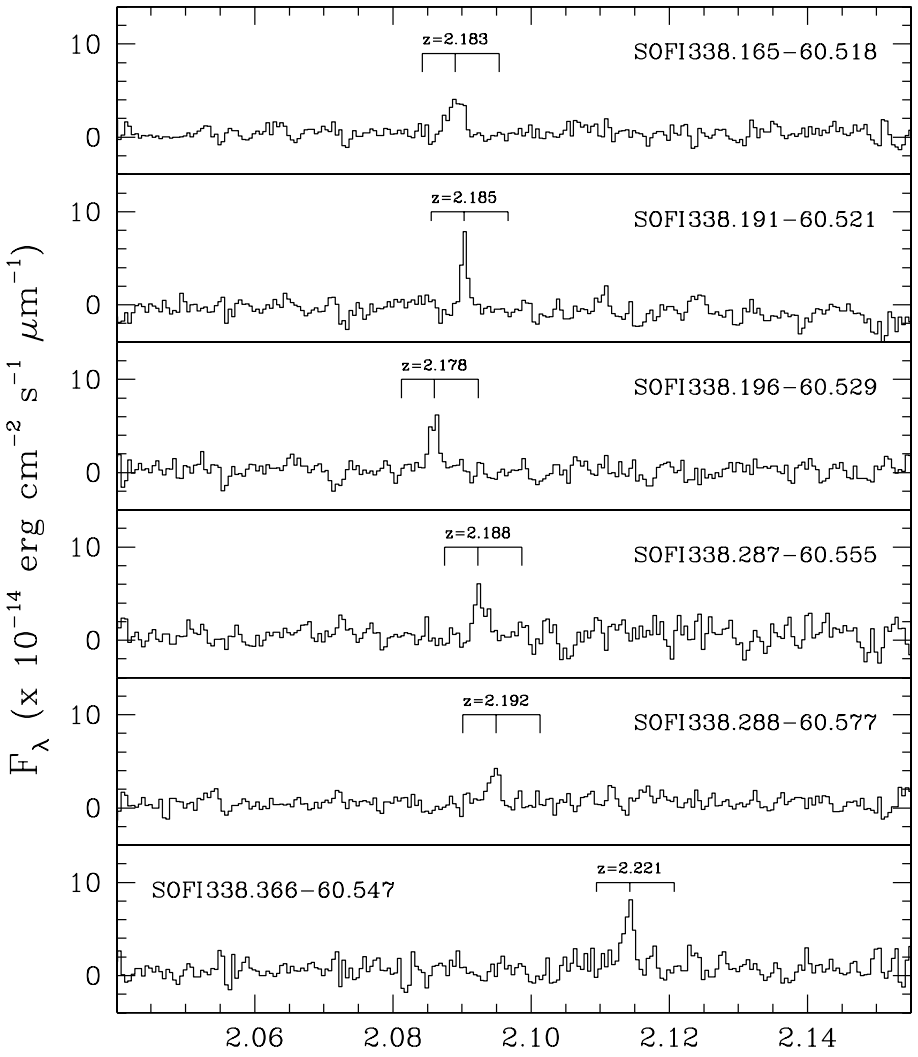

Fig. 7. ISAAC spectra of Hα emitting galaxies. The tick marks under the redshift labels show the expected positions of the [NII](6548,6584 Å) lines assuming the detected line is Hα.

than those estimated from the UV continuum. Although there are considerable uncertainties in these numbers they do support the expectation, based on the wavelength dependence of dust extinction, that extinction to the UV continuum is higher than to Hα. They are also roughly consistent with the extinction correction at this redshift most recently adopted in deriving the SFRD from the UV continua of Lyman break galaxies (Steidel et al. 1999). It is worth noting, however, that the Hα emission could actually suffer higher extinction if the youngest stars are still more heavily enshrouded in dust than those responsible for the bulk of the UV continuum. This appears not to be the case. The fact that these galaxies are detected in the rest frame UV continuum also argues against very high absolute extinction values although the possibility remains that a substantial fraction of the star formation activity could be obscured to both the UV continuum and Hα.

Table 4. Comparison of SFRs from Hα and UV continuum

Source	I[a]	L^{b}_{uv}	SFR^{c}_{uv}	$SFR^{c}_{H\alpha}$	$R(H_\alpha/uv)$
338.191–60.521	2(E)	4.6	6.5	24.3	3.7
338.196–60.529	2.8(W)	6.5	9.1	26.8	3.0
338.287–60.555	10.3(W)	23.8	33.3	24.3	0.7
338.288–60.577	5.2(W)	11.9	16.7	21.74	1.3
338.366–60.547	3.1(E)	20	28	36	1.3

[a] 10^{-19} erg cm^{-2} s^{-1}Å^{-1} (E-EIS, W-WFPC2)
[b] 10^{28} erg s^{-1}Hz^{-1} at $\simeq$ 2500 Å
[c] M$\odot$/yr

4.2. Dynamics

Despite the fact that most spectra were obtained with a 2″ slit (FWHM = 213 km s^{-1}) and the relatively low s/n ratios some of the detected emission lines are resolved and their estimated velocity dispersions given in Table 3 range up to $\simeq$ 200 km s^{-1} with a mean value $\simeq$ 80 km s^{-1}. This value is similar to that found from infrared spectroscopy of Lyman Break galaxies (Pettini 2000). Applying the formula in Devereux et al. (1987) the implied mass within the central few kpc is typically $\sim 10^{10}$M$\odot$. This of course assumes that the line widths are related to the mass and not due to the kinematics of the gas e.g winds.

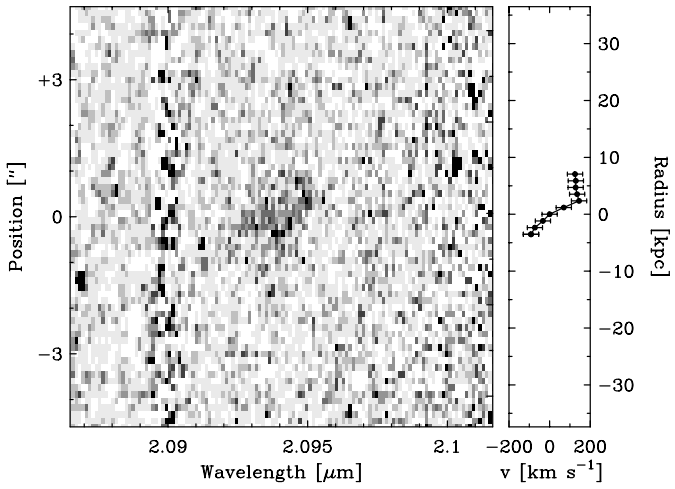

Fig. 8. The left panel is the 2D spectrum of 338.288–60.57 whose line emission is 'tilted' relative to the dispersion direction due to the galaxy rotation. The right panel is the rotation curve obtained by fitting Gaussians to the spectra at each spatial position along the slit.

The clearest evidence that we are actually observing relatively massive systems is provided by the observations of 338.288–60.577 which were made with the 1″ slit when the seeing was $\leq 0.6''$. Its HST I band image shown in Fig. 6 shows this galaxy to be extended $\simeq 1''$ in the N-S direction and aligned within $\simeq 10^{o}$ with the slit. Assuming an effective extent of 6kpc along the major axis the mass implied by the measured velocity dispersion of 117 km s^{-1} is $\simeq$ 2 x 10^{10}M$\odot$. Of more significance in this case, however, is the clear tilt of the Hα line which we attribute to ordered rotation. Although the s/n ratio is low, this is clearly evident in the 2D spectral image which is shown in Fig. 8 together with the corresponding rotation curve obtained by fitting Gaussian profiles to the emission at each spatial position along the slit. The fact that the line is tilted is robust. It appears in spectra reduced from each half of the data set independently and in a separate spectrum obtained with the 2″ slit on another night. The details of the extracted rotation curve are clearly somewhat uncertain due to the low s/n ratio. In particular, the reality of the flattening observed on the positive velocity side would need to be confirmed by higher s/n observations. The basic information of interest, however, is the observed p-p velocity spread of 247$\pm$30 km s^{-1} over a distance of 0.6″ or $\simeq$ 6kpc. The intrinsic value increases to 275$\pm$30 km s^{-1} after correction for the inclination of i = 64$\pm5^{o}$ deduced from the aspect ratio a/b = 2.15$\pm$0.3 in the I band image after correction for the PSF. Our observations thus imply a rotational velocity of 138$\pm$15 km s^{-1} at r $\simeq$ 3 kpc which may also be the terminal velocity if the observed flattening is real. This is comparable to what is seen in nearby disk galaxies whose 21 cm HI rotation curves tend to flatten at velocities in the range 100–300 km s^{-1} at radii of 1–5kpc (Begeman et al. 1991). On this evidence, therefore, it appears that well developed, massive systems were already in place at z $\simeq$ 2.

338.288–60.577 was also observed with SOFI in the EIS deep survey and has an apparent H band magnitude of 24.34 (AB) which corresponds to a rest frame absolute B magnitude of M_B = -22.4. For its FWHM Hα velocity of $\simeq$240 km s^{-1} this is about 3 magnitudes brighter than expected for a nearby galaxy falling on the Tully-Fisher relation (unless the full rotation curve extends over $\simeq$ 1000 km s^{-1} and only flattens at a radius $\geq$ 12 kpc which is highly unlikely). A similar result has been obtained for Lyman Break galaxies at z $\simeq$ 3 (Pettini 2000). Qualitatively, it is of course to be expected that these highly active star forming galaxies exhibit enhanced B luminosity to mass ratios. It is nevertheless interesting that these first quantitative estimates yield values similar to the total increase in the SFRD out to these redshifts.

4.3. Hα luminosity function

Gallego et al. (1995) have shown that the Hα luminosity function of galaxies in the local universe is well fitted by a Schechter function of the form

$$\phi(L)dL = \phi^*(L/L^*)^{\alpha}e^{-L/L^*}d(L/L^*) \quad (1)$$

with α = -1.3, ϕ^* = 6.3 x10^{-4}Mpc^{-3} and L* = 1.4 x10^{42} erg s^{-1}.

They computed the volume density of galaxies Φ(log L) per Mpc^3 per 0.4 interval of log L(Hα) where

$$\Phi(logL)(dlogL)/0.4 = \phi(L)dL \quad (2)$$

At higher redshifts in the range z $\simeq$ 0.6–1.8, Yan et al. (1999) find that the Hα luminosity function of galaxies detected in their HST NICMOS grism survey is also well fitted with a function having the same form but with

$$\phi^* = 1.7\text{x}10^{-3}\text{Mpc}^{-3}\,\text{and}\,L^* = 7\text{x}10^{42}\text{ergs}^{-1} \quad (3)$$

Between $z = 0$ and $\simeq 1$ therefore the density of Hα emitting galaxies increases by a factor 2.7 and L*(Hα) by a factor 5. The total star formation rate density thus increases by a factor of 13.5. Although this is comparable to that deduced from the UV continua of CFRS galaxies (Lilly et al. 1996) the true ratio must actually be larger as the Gallego et al. results have been corrected for extinction derived from the Balmer decrements whereas those of Yan et al. have not.

For comparison we have estimated the co-moving volume density of Hα emitting galaxies found at z = 2.2 in our survey. For each candidate galaxy in Table 2 we have computed the maximum co-moving volume V_{max} in which it could have been detected by summing the survey volumes for which the required flux sensitivity was reached. Within luminosity bins of d log L(Hα) = 0.4 we then computed

$$\Phi(logL) = \sum 1/V_{max} \quad (4)$$

For each bin the statistical errors were also computed as the square roots of the variance i.e the sum of the squares of the inverse volumes.

The results are shown in Fig. 9 where the filled squares are from the present work and the curves are the Schechter function

fits to the luminosity functions at z=0 and z$\simeq$ 1.3 given by Gallego et al. (1995) and Yan et al. (1999).

The candidates found in our survey occupy a relatively limited range in Hα luminosity - limited at the lower end by sensitivity and at the higher by area coverage. The narrow band imaging technique used to find our sources is also subject to an equivalent width threshold which increases with decreasing source flux. Estimated from the photometry, the actual rest frame EWs of our detected sources are in the range 50–700 Å whereas about 30% of the galaxies in the Gallego sample have EWs $\leq$ 50 Å. At the high luminosities detectable in our survey, however, the EW distribution can be expected to be shifted to higher values in which case this selection effect is expected to have a relatively small effect.

It is of interest that our value for the highest luminosity bin is somewhat low relative to the z $\sim$ 1.3 curve and could indicate a deficiency in extremely high star formation rate galaxies. As discussed above, such an effect may be expected if the extinction increases with SFR as found in nearby starburst galaxies. The density for the lowest luminosity bin is probably too low due to incompleteness. The nominal co-moving survey volumes given in Table 1 are for a redshift range corresponding to the FWHM of the narrow band filters. As the filters have closer to Gaussian than rectangular shapes, however, the flux limits depend on redshift within the passband. It is not possible to correct the imaging data directly for this because the line wavelengths and hence true fluxes are not known *a priori*. Estimates of this effect have been made, therefore, using the measured transmission curves of the narrow-band filters. For the 2.09 μm filter the nominal Δz corresponding to the FWHM is 0.03. For the flux limit reached in the WFPC field the effective Δz for 3σ detections decreases from 0.038 to 0.027 for objects with log L(Hα) = 43 to 42.4 but falls to 0.0085 at log L(Hα) = 42.2. For the 2.12 μm filter, with a nominal Δz =0.043, the effective values on the same field decrease from 0.06 to 0.027 in the range log L(Hα) = 43 to 42.4 and is essentially 0 at 42.2. For these fields therefore the conclusion is that errors in the volume densities are relatively small for log L(Hα) $\geq$ 42.4 but can be large at lower luminosities.

As not all candidates in the survey have been spectroscopically confirmed it is also possible that the plotted points are actually too high. As a check, therefore, we have computed separately the volume density of the spectroscopically confirmed candidates in the WFPC2.09 field. As all of these objects have log L(Hα) in the range 42.4–42.6, the effective co-moving volume expected is very close to the nominal one adopted based simply on the FWHM of the NB filter. As objects with log L(Hα) = 42.4 are brighter than the flux limit in this field the detections at this luminosity should also be complete. In fact the volume density of log Φ = -2.5 (+0.17,-0.25) obtained is a factor 2 higher than the value of -2.8 (+0.14,-.22) derived from the complete imaging survey. This is actually not surprising given that this field is the deepest and appears to contain a small group or cluster. Despite that, the magnitude of the effect is actually only at the level of the quoted statistical uncertainties. Within these uncertainties, our overall conclusion is that the comparison of our result with that of Yan et al. is consistent with either no or only modest evolution in the Hα luminosity function between $z \simeq 1.3$ and 2.2.

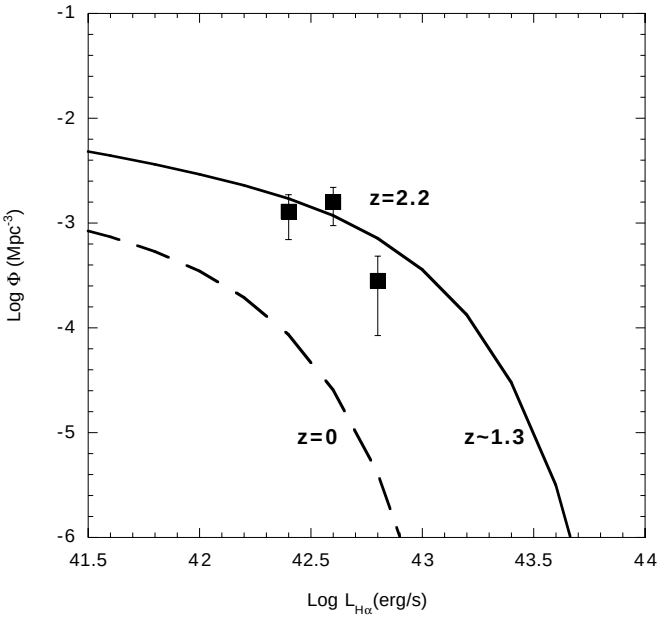

Fig. 9. Hα luminosity functions. The filled squares are from this work and correspond to the assumption that all survey candidates detected at $\geq$ 3 σ are real. The curves are the best fit Schechter functions to the data of Yan et al. (1999) at z $\sim$ 1(solid) and those of Gallego et al. (1995) at z=0 (dashed).

4.4. Star formation rate density

The total Hα luminosity density at z= 2.2 can be estimated by integrating the Schechter function

$$L_{tot}(H\alpha) = \int \phi(L) L dL = \phi^* L^* \Gamma(2+\alpha) = 1.3\phi^* L^* \quad (5)$$

As we cannot improve on the fit provided by the curve of Yan et al. we use this to obtain L$_{tot}$(Hα) = 1.55x10^{40} erg s^{-1}. To convert this to a star formation rate density we then use the relation SFR(M$_\odot$yr^{-1}) = 7.9x10^{-42}L(Hα)(erg s^{-1}) from Kennicutt (1998) which yields a SFRD = 0.12 M$_\odot$ yr^{-1}. This is, of course, identical to the Yan et al. value at z $\sim$1 and the implied flatness of the SFRD vs z curve in this range is independent of extinction as no correction has been applied in either case. It is of interest to note that our value of the SFRD is also almost identical to that derived by Steidel et al. (1999) from extinction corrected UV continuum measurements of galaxies at z $\sim$3–4.5. This direct comparison is not strictly fair as Steidel et al. (1999) imposed a cut-off at 0.1 L* which could lead to a factor $\simeq$ 2 underestimate in the total SFRD. On the other hand, correction for extinction would also lead to some increase in our value. It is important to stress here, however, that agreement at this level is remarkable enough given the small size of our sample, issues of completeness and the large uncertainties in the shape of the adopted luminosity function.

5. Conclusions

- A 2.1 μm narrow band imaging survey conducted with SOFI at the ESO NTT has yielded about 10 candidate Hα emitting galaxies with fluxes down to a few x 10^{-17} erg cm^{-2} s^{-1} over an area of 100 arcmin^2 which includes the HDFS WFPC2 and STIS fields.
- Based on HST WFPC2 observations of the HDFS flanking fields only one of these objects appears to be an interacting system with 3 components within $\sim$ 10kpc. Three objects appearing in EIS Deep images of the HDFS exhibit extremely red U-B colours, consistent with Lyman forest absorption at the target redshift of z = 2.2
- Six of the best candidates have been confirmed spectroscopically using ISAAC at the ESO VLT. Although only a single emission line is seen in each case its only plausible identification is Hα. Absence of the [NII]$\lambda\lambda$6548,6584 lines is consistent with the high [OIII]/Hβ ratios observed on higher redshift Lyman Break galaxies and indicative of high ionization and/or low metallicity systems. This is the largest sample of spectroscopically confirmed, high redshift, galaxies selected by narrow band infrared imaging.
- Star formation rates derived from the Hα fluxes are in the range 20–35M$\odot$/yr without extinction correction and are, on average, a factor $\sim$ 2 higher than those derived from the UV continua of the same galaxies.
- The velocity dispersions $\sim$ 100 km s^{-1} are similar to those measured in Lyman Break galaxies and imply masses $\sim 10^{10}$M$\odot$ provided they are related to mass and not winds. More direct evidence that these are relatively well developed systems is provided by a rotation curve obtained for one galaxy which yields a rotational velocity of $\simeq$ 140 km s^{-1} at a radius of 3 kpc which is comparable with nearby disk galaxies. The absolute B magnitude of this galaxy is $\simeq$ 3 magnitudes brighter than expected from the local Tully-Fisher relationship.
- Although sampling only a narrow range around log L(Hα) $\simeq$42.6, comparison of our data with the results of the Hα NICMOS grism survey conducted by Yan et al. (1999) imply little or no evolution in the Hα luminosity function and hence of the Star Formation Rate Density between z $\sim$1.3 and 2.2.
- Our best estimate of 0.12 M$\odot$ yr^{-1}Mpc^{-3} for the SFRD at z =2.2 is, within the statistical uncertainties, equal to that derived from the UV continuum flux of Lyman Break galaxies at z = 3–4.5 by Steidel et al. (1999).
- Additional spectroscopy covering Hβ and [OIII]λ4959,5007 is now planned in order to measure the extinction and estimate the metal abundances in these systems.

Acknowledgements. We are grateful to Max Pettini and Lin Yan for helpful discussions.

References

Beckwith S.V.W., Thompson D., Mannucci F., Djorgovski S.G., 1998, ApJ 504, 107
Begeman K.G., Broeils A.H., Sanders R.H., 1991, MNRAS 249, 523
Bertin E., Arnouts S., 1996, A&AS 117, 393
Devereux N.A., Becklin E.E., Scoville N., 1987, ApJ 312, 529
Gallego J., Zamorano J., Aragón-Salamanca A., Rego M., 1995, ApJ 455, L1
Gallego J., Zamorano J., Rego M., Vitores A.G., 1997, ApJ 475, 502
Genzel R., Lutz D., Sturm E., et al., 1998, ApJ 498, 579
Glazebrook K., Blake C., Economou F., Lilly S., Colless M., 1999, MNRAS 306, 843
Iwamuro F., Motohara K., Maihara T., et al., 2000, PASJ in press, astro-ph/0001050
Kennicutt R.C., 1983, ApJ 272, 54
Kennicutt R.C., 1998, ARA&A 36, 189
Lilly S.J., Le Fèvre O., Hammer F., Crampton D., 1996, ApJ 460, L1
Madau P., Ferguson H.C., Dickinson M.E., et al., 1996, MNRAS 283, 1388
Mannucci F., Thompson D., Beckwith S.V.W., Williger G.M., 1998, ApJ 501, L11
Moorwood A.F.M., Cuby J.G., Lidman C., 1998, The Messenger 91, 9
Moorwood A.F.M., Cuby J.G., Ballester P., et al., 1999, The Messenger 95, 1
Pettini M., Kellog M., Steidel C., et al., 1998, ApJ 508, 539
Pettini M., 2000, Phil. Trans. R. Soc. London, Ser. A in press (astro-ph/0001075)
Steidel C.C., Adelberger K.L., Giavalisco M., Dickinson M., Pettini M., 1999, ApJ 519, 1
Teplitz H.I., Malkan M., McLean I.S., 1998, ApJ 506, 519
Thompson D., Mannucci F., Beckwith S.V.W., 1996, AJ 112, 1794
Tresse L., Maddox S.J., 1998, ApJ 495, 691
van der Werf P.P., Moorwood A.F.M., Bremer M.N., 2000, A&A in press
Williams R.E., Baum S., Bergeron L.E., et al., 2000, AJ in press
Yan L., McCarthy P.J., Freudling W., et al., 1999, ApJ 519, L47